Journal of Molecular Liquids 315 (2020) 113606

Contents lists available at ScienceDirect

Journal of Molecular Liquids

journal homepage: www.elsevier.com/locate/molliq

First-principles molecular dynamics studying the solidification of Ti-6Al-4V alloy

Jia Song [a], Luyu Wang [b], Liang Zhang [a,*], Wenheng Wu [a], Zhibin Gao [c,*]

[a] Shanghai Engineering Research Center of 3D Printing Materials, Shanghai Research Institute of Materials, Shanghai 200437, China
[b] Institute of Fiber-Based New Energy Materials, The Key Laboratory of Advanced Textile Materials and Manufacturing Technology of Ministry of Education, College of Materials and Textiles, Zhengjia Sci-Tech University, Hangzhou 310018, China
[c] Department of Physics, National University of Singapore, Singapore 117551, Republic of Singapore

ARTICLE INFO

Article history:
Received 28 April 2020
Received in revised form 4 June 2020
Accepted 13 June 2020
Available online 25 June 2020

Keywords:
First-principles molecular dynamics
Ti-6Al-4V alloy
Structural evolution
Transport property

ABSTRACT

Solidification process plays a significant role in macroscopic properties of metallic materials. However, the understanding of this process at the atomic level is still far from complete. In this work, for the first time, the first-principles molecular dynamics simulations are carried out to systematically explore the structural evolution and transport properties of Ti-6Al-4V alloy, one of the commonly used alloys for selective laser melting technology, upon cooling from 2400 K to 1300 K. Firstly, the melting range of this alloy is predicted by simulated density to be about 1850–1950 K, which is in good agreement with the experimental value of 1875–1925 K. Afterwards, the local atomic structure variation with temperature is statistically analyzed by structure factors, partial radial distribution functions, coordination number, bond angle distributions, and Voronoi tessellation. It reveals that Ti-6Al-4V alloy experiences a phase transition from 2400 K to 1300 K. The system changes from a liquid dominated by the icosahedral-like cluster to a solid with body-centered cubic structure, where the ⟨0, 5, 2, 6⟩ and ⟨0, 4, 4, 6⟩ polyhedra play an important role. Eventually, the diffusion coefficients of Ti, Al, and V are estimated to investigate the kinetic property of liquid Ti-6Al-4V alloy. From 2400 K to 1950 K, the diffusion coefficients of atoms all obey Arrhenius function, and V atom has the largest diffusion coefficient, followed by the Ti atom, which is very close to the self-diffusion coefficient of pure liquid Ti, and finally the Al atom. This abnormal mass dependence of diffusion coefficient is well explained by activation energy. In conclusion, the present work provides insights into the understanding of structural dynamics and the kinetic properties of such alloy melts, which could guide selective laser melting technology to obtain desired microstructure.

1. Introduction

Solidification process, a common phenomenon in nature, has an important influence on the properties of materials, especially metals. This is because the macroscopic properties of metallic materials are essentially determined by their various microstructures, which in turn are extremely affected by the initial state of melt and various external conditions during the solidification process [1–6]. Therefore, it is necessary to have a very clear understanding of the evolution mechanism of the microstructure during the solidification process, so that it is possible to control the evolution and formation of the microstructure by changing the initial state of the melt or external conditions and then obtain the desired microstructure. However, metal solidification is a complicated process [7], involving the conduction of heat and mass, the release of latent heat, beginning and continuous growth of crystal structure and so on, which is difficult to directly observe from traditional experiments because the temperature of the metal solidification process is generally high and the time is extremely short.

Nowadays, computer simulation has become a bridge between the theory and experimental research of metal solidification, especially in areas where the current experimental conditions cannot be reached. Molecular simulations have brought a lot of valuable data and conclusions to the investigation of the solidification process, which has greatly promoted our understanding of the solidification principle and controlling the solidification process. Xiong et al. [8] studied the structural properties of liquid $Ag_{74}Ge_{26}$ alloy at multiple temperatures by ab initio molecular dynamics simulation. They found that a highly dominated short-range order associated with the nearest-neighbors shell could improve the development of medium-range order and the formation of metallic glasses. Debela et al. [9] simulated the structural evolution of liquid niobium from 3000 to 1500 K and found that abundant icosahedra existed in the liquid and undercooled liquid, which symbolized the existence of numerous precursor phases in the liquid melt at low temperature, especially body-centered cubic (bcc) structure. By using

* Corresponding authors.
E-mail addresses: lzhang0126@hotmail.com (L. Zhang), zhibin.gao@nus.edu.sg (Z. Gao).

https://doi.org/10.1016/j.molliq.2020.113606
0167-7322/

ab initio molecular dynamics simulation to research the transport properties and Stokes-Einstein relation in liquid Al alloying with elements Ni, Cu, and Zn, respectively, Jakse et al. [10] found that the competition between local icosahedral ordering and local chemical ordering may cause the breakdown of the Stokes-Einstein relationship even in metallic melts, which provided a unique framework to study the relationship between structure, thermodynamics, and dynamics in liquid alloy.

Ti-6Al-4V alloy is an $\alpha + \beta$ titanium alloy with approximately 6 wt% Al stabilizing the α phase and 4 wt% V stabilizing the β phase. The α-Ti is a hexagonal close-packed (hcp) structure and β-Ti is a bcc structure. Due to the special structure of Ti-6Al-4V alloy, it has excellent property and is widely used in many fields, such as biomedicine and aerospace [5]. Besides, it is also one of the commonly used alloys for selective laser melting (SLM) technology [6]. When we talk about SLM of Ti-6Al-4V alloy, the process of alloy melting and solidifying must be investigated. Unfortunately, there is almost no any molecular dynamics simulations about Ti-6Al-4V alloy melting and solidifying, only the molecular dynamics simulations of other titanium alloys, such as Xia et al. [3] simulating the rapid quenching process of pure Ti, Zhang et al. [11] researching the phase transformation of Ti—Al alloy with low Al content, Shimono et al. [12] studying the formation and crystallization of Ti—Al amorphous alloys, Fujinaga et al. [13] investigating the nucleation dynamics in Al solidification with Al—Ti refiners, and Li et al. [14] revealing the structural evolution of TiAl during rapid solidification processing.

To sum up, this paper aims to explore the structural evolution and dynamical properties of Ti-6Al-4V alloy in a temperature range between 2400 K and 1300 K via first-principles molecular dynamics (FPMD) simulations. The simulated density of the alloy is calculated first at different temperatures and validated by experimental values. Moreover, the structural evolution from FPMD simulation is statistically analyzed by using structure factor, partial radial distribution function (PRDF), coordination number (CN), bond angle distribution function (BADF), and Voronoi tessellation. In the end, the dynamical properties of liquid Ti-6Al-4V alloy are discussed via diffusion coefficients and viscosity.

2. Methodology

2.1. Density functional theory calculations

FPMD simulations of the Ti-6Al-4V alloy are performed by the Vienna Ab-Initio Simulation Package (VASP) [15–18]. The generalized gradient approximation (GGA) in the form of Perdew-Burke-Ernzerhof (PBE) functional is used to treat the exchange-correction energy of the electron [19,20]. The wave functions of valence electrons, Ti ($3p^6 3s^2 4p^2$), Al ($3s^2 3p^1$) and V ($3p^6 3d^3 4s^2$), are expanded in the plane-wave basis set with a cutoff energy of 500 eV [21], which is roughly 1.3 times higher than the default value. The core electrons are approximated by Projector-Augmented-Wave (PAW) pseudopotentials [22]. In FPMD simulations, the equation of motion is solved through the velocity algorithm with a time step of 3 fs. The energy convergence criterion of the electronic self-consistency is set to 10^{-6} eV per atom. The spin polarization is always applied for all FPMD simulations to properly depict the unpaired electrons in valent shells [15].

In this study, the simulated Ti-6Al-4V alloy is comprised of 110 Ti atoms, 14 Al atoms, and 4 V atoms with approximate mass fractions of Ti, Al, and V at 0.90, 0.06 and 0.04. All simulation cells are cubic with a periodic boundary to eliminate boundary effects. Only the Γ point is considered to sample the Brillouin zone of the supercells in the simulations [23]. The initial configuration of Ti-6Al-4V is fully melted at 2400 K, much higher than the experimental melting point value of 1943 K of pure Ti [24], to remove the crystalline symmetry, followed by stepwise cooling to 2200, 2000, 1950, 1850, 1800, 1700, 1500, and 1300 K. At each temperature, 5000 steps (15 ps) of simulations are carried out in the NPT ensemble (constant number, pressure, and temperature) with a Langevin thermostat and a Parrinello-Rahman barostat controlling temperature and pressure to optimize the cell volumes of Ti-6Al-4V alloy [25,26]. The cell volumes are evaluated as the average between 9 ps and 15 ps of simulations and used as input structure in the following NVT ensemble simulations (constant number, volume, and temperature) with a Nosé-Hoover thermostat controlling temperature [26]. In the NVT ensemble, the structural relaxation continues for 10,000 steps to reach thermal equilibrium. Afterward, an additional 4000 FPMD steps in the NVT ensemble are used for the analysis of the structural and dynamical properties.

3. Results and discussion

3.1. The density of the Ti-6Al-4V alloy

Density is an essential property of a material. Generally, the density differs greatly between different states, for instance, density jump near the melting point. Fig. 1 shows both the simulated densities evaluated from the equilibrium volume and experimental densities originated from previous reports. The density calculated from FPMD simulations increases from 4.038 to 4.356 $g \cdot cm^{-3}$ as the temperature decreases from 2400 to 1300 K. Meanwhile, the corresponding experimental density, as suggested by Li et al. [24], decreases from 4.006 to 4.363 $g \cdot cm^{-3}$. Our FPMD density is close to the experimental density with the absolute deviation between 0.09% and 0.80%, reflecting a good description of interatomic interaction in the Ti-6Al-4V alloys by PBE functional. The temperature dependence of density can be fitted satisfactorily to a linear relationship at different temperature ranges,

$$\rho = a - bT \tag{1}$$

In the temperature range of 1850–1300 K, a and b are parameters evaluated from experimental density at 4.600 $g \cdot cm^{-3}$ and 1.828×10^{-4} $g \cdot cm^{-3} \cdot K^{-1}$, and from FPMD density at 4.565 $g \cdot cm^{-3}$ and 1.590×10^{-4} $g \cdot cm^{-3} \cdot K^{-1}$, respectively; In the temperature range of 2400–1950 K, parameters a and b evaluated from experimental density are 4.620 $g \cdot cm^{-3}$ and 2.557×10^{-4} $g \cdot cm^{-3} \cdot K^{-1}$, and from FPMD density are 4.616 $g \cdot cm^{-3}$ and 2.409×10^{-4} $g \cdot cm^{-3} \cdot K^{-1}$.

Compared with the experimental results, at $T \geq 1950$ K, the simulated density clearly belongs to the liquid branch, and at $T \leq 1850$ K, the simulated density distinctly belongs to the solid branch. In addition, it is worth noting that the simulated density of Ti-6Al-4V alloy drops sharply from 1850 to 1950 K. This phenomenon can be attributed to the melting of the system. Therefore, the temperature range from 1850 to 1950 K corresponding to density jump in the density-

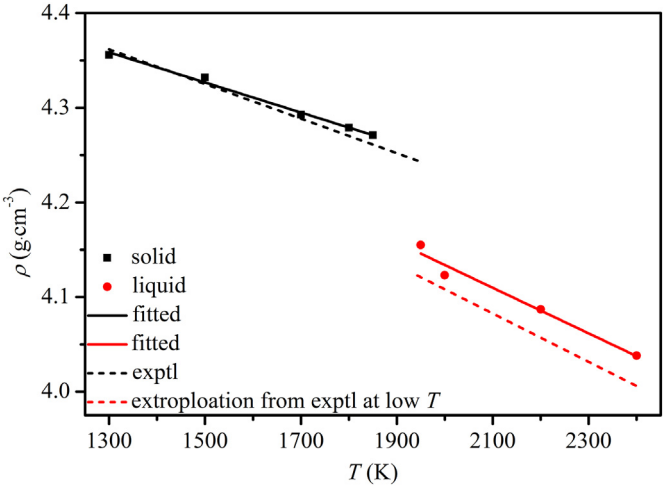

Fig. 1. The FPMD and experimental densities of Ti-6Al-4V alloy as a function of temperature.

temperature curve is defined as the theoretical melting range of the Ti-6Al-4V alloys, extremely consistent with the melting range from 1873 to 1923 K (Goodfellow Cambridge Ltd. data) measured from the experiment [27]. It is concluded that the method of simulating density used in this study is reasonable.

3.2. Structure factor

The total structure factor, $S(q)$, is calculated by the Faber-Ziman formalism [28],

$$S(q) = \frac{a_\alpha^2 f_\alpha^2 [S_{\alpha\alpha}(q)-1] + 2a_\alpha a_\beta f_\alpha f_\beta [S_{\alpha\beta}(q)-1] + a_\beta^2 f_\beta^2 [S_{\beta\beta}(q)-1]}{\left(a_\alpha f_\alpha + a_\beta f_\beta\right)^2} \quad (2)$$

in which a_α (or a_β) is the atomic density of corresponding species, f_α (or f_β) is neutron scattering length of corresponding species, and $S_{\alpha\beta}(q)$ is partial structure factors. Fig. 2 illustrates the total structure factor of Ti-6Al-4V alloy from 2400 to 1300 K. As temperature decreases, the main peaks of $S(q)$ become narrower, their peak values gradually shift to the right, and their amplitudes increase. These phenomena indicate that short-range order (SRO) increases during the solidification of Ti-6Al-4V alloy. The second peaks of $S(q)$ can be applied to characterize different types of SRO in the liquid, for example, a shoulder on the high q side of the second peak is a signature of icosahedron. From inset of Fig. 2, it can be seen that the shoulder of the second peak near 5.25 $Å^{-1}$ becomes more pronounced from 2400 to 1950 K. Taking the position of the main peak as q_{main} and that of second peak and shoulder as q_{second} and q_{shoulder}, the $q_{\text{second}}/q_{\text{main}}$ and $q_{\text{shoulder}}/q_{\text{main}}$ are calculated to be approximately 1.74 and 1.98 at 1950 K, respectively, corresponding to the ideal icosahedron [9]. To further investigate the local structure evolution of Ti-6Al-4V alloy during cooling, we will discuss PRDF, BADF, and Voronoi tessellation in the following sections.

3.3. Partial radial distribution function and coordination number

The partial radial distribution function (PRDF) is the most important structural information obtainable from FPMD simulations. It is defined as follows,

$$g_{\alpha\beta}(r) = \frac{V}{N_\alpha N_\beta} \left\langle \sum_{\alpha=1}^{N_\alpha} \frac{n_{\alpha\beta}(r,\Delta r)}{4\pi r^2 \Delta r} \right\rangle \quad (3)$$

where V is the volume of the supercell, α is the central atom, β is the coordination atom, N_α and N_β are the numbers of α and β atom in the supercell, $n_{\alpha\beta}(r, \Delta r)$ is the number of β species in the sphere shell from r to $r + \Delta r$, and the symbol $\langle\cdots\rangle$ represents the time average.

Due to the low content of V atoms in this ternary alloy, the PRDF of V—V lacks statistical significance and is thus not considered in the present work. Fig. 3 shows the PRDFs of Ti—Ti, Ti—Al, Ti—V, Al—Al, and Al—V couples at different temperatures. Our calculated PRDF of Ti—Ti has an acceptable agreement with previous MD simulations reported by Xia et al. [3]. It indicates that our simulations are reasonable. In the temperature range of 2400–1950 K, all PRDFs show an obvious first peak, visible second peak, and weak third peak, which is the common behavior of liquids at high temperatures. The amplitude of these peaks grows bit by bit with temperature decreasing. At 1850 K, the first peak suddenly becomes intense, the second and third peaks both split into two peaks and a small peak appear at about 6.5 Å, suggesting that this alloy reaches a higher extent of SRO, and a significant structural transition most likely occurs at 1850 K [9]. As temperature further goes down, the characteristic peaks of each PRDF become amplified and coincide with that of bcc structure from 1850 to 1300 K [4], that is, Ti, Al, and V atoms are arranged according to the bcc structure in this temperature range. The last interesting finding is that the first peak of $g_{\text{AlV}}(r)$ tends to become much sharper with decreasing temperature as compared with those of $g_{\text{TiTi}}(r)$, $g_{\text{TiAl}}(r)$, $g_{\text{TiV}}(r)$, and $g_{\text{AlAl}}(r)$ in the solid. This observation is indicative of a preferred neighboring of Al—V couple over the others [29]. Therefore, it is probable that Al—V interaction would play a more important role in determining the local structure of solid Ti-6Al-4V alloy.

From the PRDFs, the coordination number (CN), $N_{\alpha\beta}$, can be estimated from the relation,

$$N_{\alpha\beta} = 4\pi \int_0^{r_{min}} r^2 a_\beta g_{\alpha\beta}(r) dr \quad (4)$$

in which a_β is the atomic concentration of species β, and r_{min} is the cut-off distance, determined by the first-minimum position of $g_{\alpha\beta}(r)$, here $r_{\text{min}} = 3.9$ Å. Figs. 4a-c demonstrate the distributions of atomic clusters versus temperature. At $T \geq 1950$ K, the CNs of Al- and Ti-centered clusters dominate in 11–14, while the V-centered clusters prefer a lower CN between 10 and 13. From 2400 to 1950 K, the percentage of CN = 12 decreases from 26.05% to 22.63% for Ti-centered cluster and keeps constant values of 31% for Al-centered cluster and 27% for V-centered cluster. Since one of the prerequisites for an atom to form an ideal icosahedron is that it should have 12 adjacent atoms, the high percentage of CN = 12 on the Al-centered cluster provides a good foundation for ideal icosahedral formation. At $T \leq 1850$ K, the Al-, Ti-, and V-centered clusters prefer a CN between 13 and 14, and the sum of fractions of the two CNs is above 90%. Because the CNs of perfect and defective bcc structure are 14 and 13, it can be speculated that there are plentiful bcc structures in the system after 1850 K. As temperature drops, the fraction of CN = 13 decreases while that of CN = 14 increases for all clusters, meaning that the defective bcc structure may transform to a perfect bcc structure during the process of continuous cooling.

Fig. 4d shows the total CN (N_α^{tot}) of each atom and the internal energy (E) versus temperature during the solidification process of liquid Ti-6Al-4V alloy. Overall, the N_{Ti}^{tot} is the largest, followed by N_{Al}^{tot} and then N_V^{tot}, compatible with the order of atomic Goldschmidt radii, r_{Ti} (1.46 Å) > r_{Al} (1.43 Å) > r_{V} (1.34 Å). Larger atoms possess more neighbor space to accommodate more atoms. From 2400 to 1950 K, the N_α^{tot} linearly varies between 12.97–13.19, 12.37–12.61, and 11.36–11.73 for Ti, Al, and V, respectively. This is because the internal energy of the system increases with temperature increasing, as shown in Fig. 4d, namely, the atoms become freer at high temperatures, resulting in a reduction in the number of atoms participating in the coordination. Afterward, the total CNs of Ti, Al, and V jump to 13.93, 13.71, and 13.23 at temperature 1850 K, and the corresponding internal energy decreases to −7.1865 eV/atom. Further lowering the temperature from 1850 to

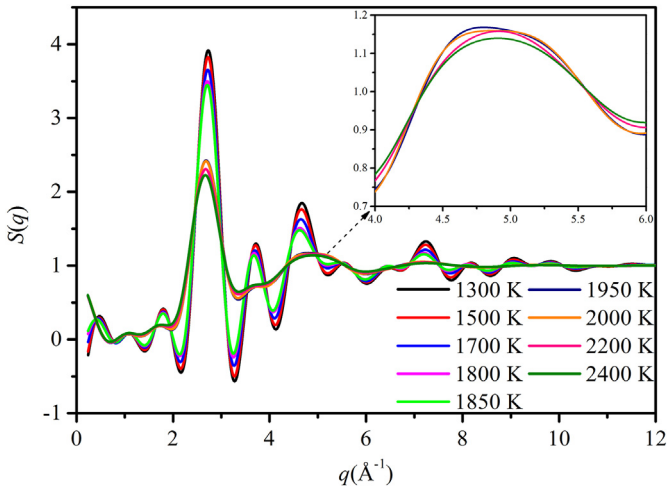

Fig. 2. The structure factor, $S(q)$, in Ti-6Al-4V alloy at multiple temperatures.

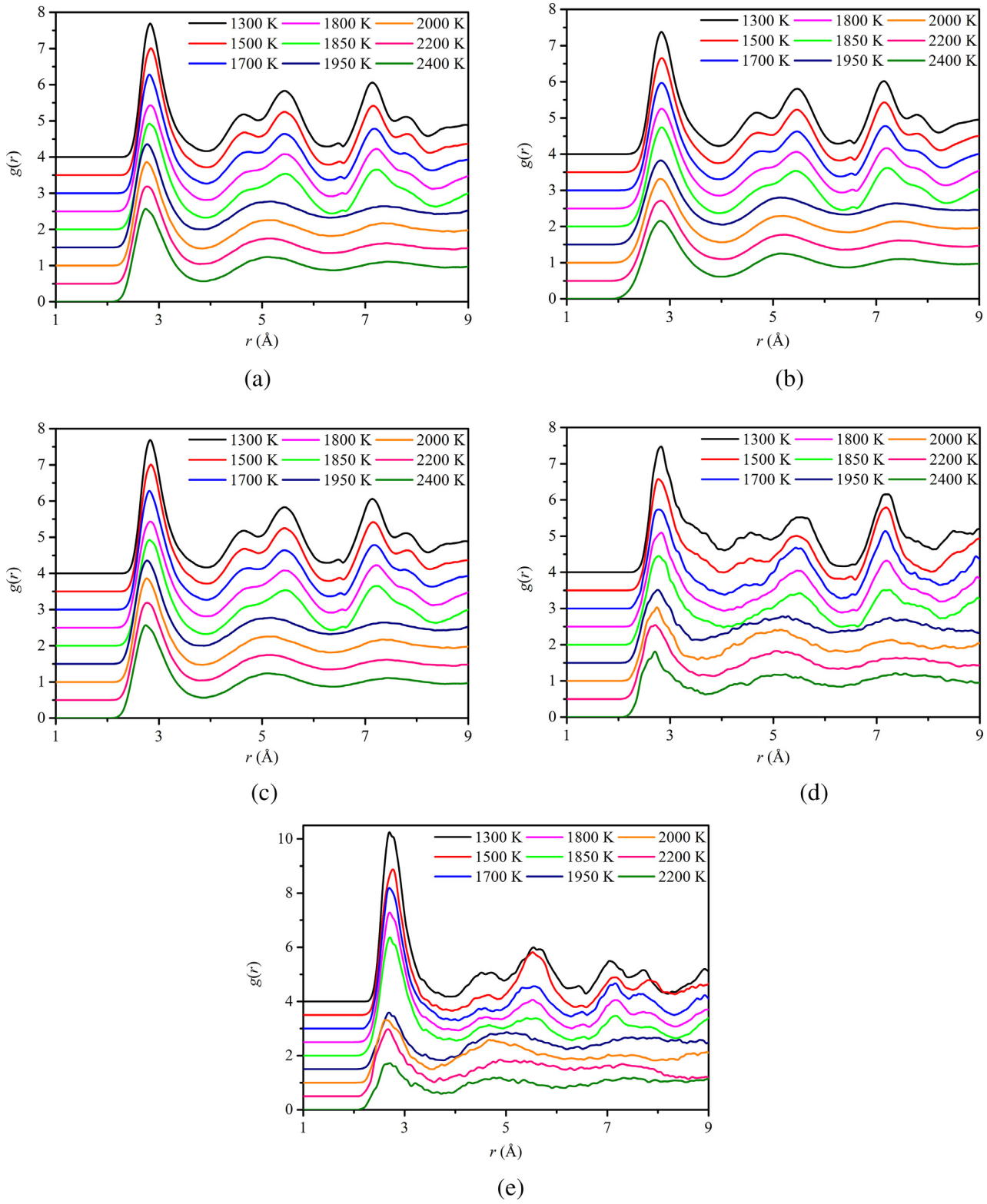

Fig. 3. The PRDFs of (a) Ti—Al, (b) Ti—Ti, (c) Ti—V, (d) Al—Al, and (e) Al—V couples at different temperatures. (Note that, for clarity, each curve has been vertically displaced from the curve below.)

1300 K, the total CNs of Ti, Al, and V maintain constant values of about 13.95, 13.83, and 13.39.

3.4. The bond angle distribution function

The bond angle distribution function (BADF), $g_3(\theta)$, is a three-body distribution function, which is defined for the angle between the nearest neighboring two atoms around a central atom within the

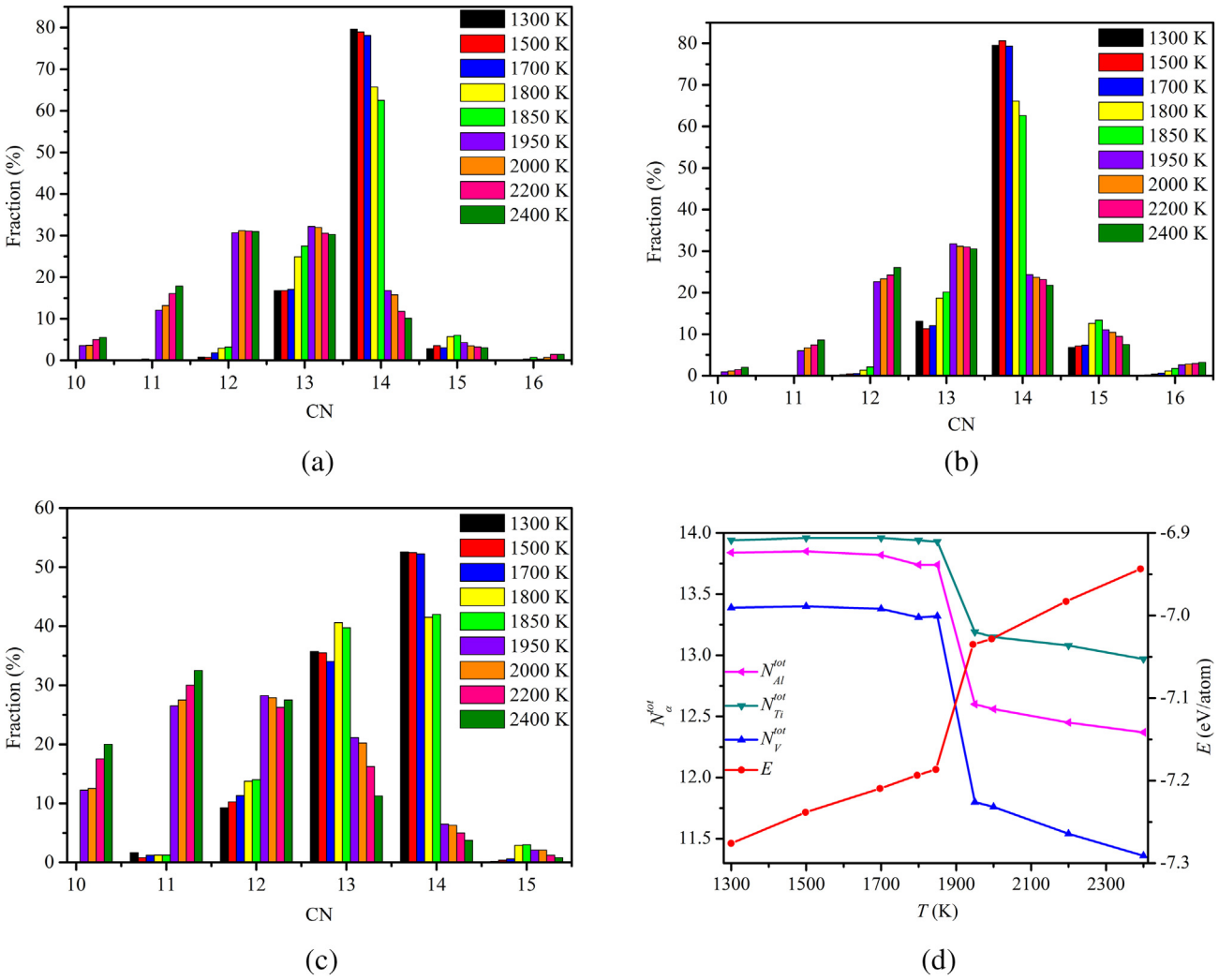

Fig. 4. Distribution of (a) Al-, (b) Ti-, and (c) V-centered cluster at different temperatures. (d) The total CN (N_{α}^{tot}) for each atom and the internal energy (E) versus temperature during the solidification process of liquid Ti-6Al-4 V alloy.

maximum bond length r_{min}. As mentioned before, the V—V couple lacks statistical significance, therefore Ti-V-V triple is also not considered in the present work. Using the bond-length cutoff of 3.9 Å, the first minimum position in the PRDFs, the BADFs of the Ti-Al-(Al, Ti, V), Ti-Ti-(Al, Ti, V) and Ti-V-(Al, Ti) triples at different temperatures are estimated and illustrated in Fig. 5. More detailed microstructure information can be obtained, at $T \geq 1950$ K, all BADFs show two prominent peaks, the first peak is near 58°, the second peak is near 108°. The peak at 58°-corresponds to the close-packed structure of liquid alloy, and the peak at 108° means that complex anisotropic local structures or incomplete tetrahedral cells remain in liquid Ti-6Al-4V alloy [3,9,30]. The positions of the two peaks are not far from the BADFs of perfect icosahedron (63.5° and 116.5°), indicating the presence of abundant icosahedra in the liquid Ti-6Al-4V alloy [9]. As the temperature decreases, the two peaks become narrower, meaning that the structure of the liquid atom becomes more ordered, and their positions gradually move towards 55° and 125° which are the characteristic peaks of bcc structure [9]. When the temperature drops to 1850 K, all BADFs present four peaks, which are located at about 55°, 90°, 120°, and 170. Peaks at 55°and 120° correspond to the close-packed structure of solid alloy, a peak at 90° corresponds to a regular octahedral and a peak at 170° corresponds to the spiral chain structure, implying that the Ti-6Al-4V alloy forms more local structures and undergoes complicated structural transformations during the cooling process. In addition, these peak positions from our FPMD simulations are extremely consistent with that of the bcc structure reported by Debela et al. [30]. Thus, it can be speculated that the disorder-to-order (liquid-to-bcc-like) phase transition of Ti-6Al-4V alloy occurs from 1950 K to 1850 K.

3.5. Voronoi tessellation analysis

The local atomic packing in Ti-6Al-4V is further explored by Voronoi tessellation analysis, which is a three-dimensional approach and can provide a more complete geometrical construction of a central atom with is neighboring atoms [31]. The Voronoi polyhedron (VP) is described by indices $<n_3, n_4, n_5, n_6>$, in which n_i is the number of faces with i edges, and the total number of faces of a VP is equivalent to the coordination number of a central atom, $\sum n_i = CN$. The standard Voronoi indices of bcc, face-centered cubic (fcc), and icosahedron are $\langle 0, 6, 0, 8\rangle$, $\langle 0, 12, 0, 0\rangle$, and $\langle 0, 0, 12, 0\rangle$.

Fig. 6 shows the top 16 most populated Voronoi indices in liquid Ti-6Al-4V alloy during solidification. As previously reported in the literature, the preference of a polyhedron depends on the solute-to-solvent radius ratio, R^*. With decreasing R^*, the preferred polyhedra can change from a Frank-kasper polyhedron ($R^* > 1.2$) to an icosahedron ($R^* < 0.902$), then to a bi-capped square Archimedean antiprism polyhedron ($R^* < 0.835$), and finally to a tricapped trigonal prism packing type polyhedron ($R^* < 0.732$) [9,32,33]. For the ternary Ti-6Al-4V alloy, the

0.888 (V/Ti) < R^* < 1.021 (Al/Ti) predicts that the icosahedron predominates in liquid state. In the liquid state, the clusters tend to form polyhedra with Voronoi indices ⟨0, 4, 4, 3⟩ (D11), ⟨0, 3, 6, 2⟩ (C11), ⟨0, 2, 8, 1⟩ (B11), ⟨0, 0, 12, 0⟩ (Z12), ⟨0, 4, 4, 4⟩ (D12), ⟨0, 3, 6, 3⟩ (C12), ⟨0, 2, 8, 2⟩ (B12), ⟨0, 4, 4, 5⟩ (D13), ⟨0, 2, 8, 3⟩ (B13), ⟨0, 1, 10, 2⟩ (A13), ⟨0, 3, 6, 4⟩ (C13), ⟨0, 3, 6, 5⟩ (D14) and ⟨0, 2, 8, 4⟩ (B14), in which the symbols in the brackets are obtained according to the method reported by Wu et al. [34]. From 2400 to 1950 K, Z12, perfect icosahedron, rises from about 2.3% to almost 4.2%, D11, C11, B11, C12, B12, and A13 are representatives of distorted icosahedra [9,32] and the sum of fractions of these clusters decreases from 42.0% to 27.9%, and the C13, C14, and B14 are classified as deformed bcc structure [35] and the sum of fractions of these clusters slightly increases from 11.7% to 15.0%. These results state that the liquid Ti-6Al-4V alloy is mainly composed of icosahedral-like local atomic structures. At T = 1850 K, the icosahedral-like clusters go down dramatically, and tend to be 0 with a further decrease of temperature. However, the Voronoi indices ⟨0, 5, 2, 6⟩ (E13), ⟨0, 4, 4, 6⟩ (D14) and ⟨0, 6, 0, 8⟩ (F14) suddenly occur at 1850 K, approximately 9.1%, 7.5% and 34.1%, respectively. The populations of E13 and D14 increase at the beginning of the crystallization process but other polyhedra except F14 drop, indicating the E13 and D14 play an important role in the crystallization process of Ti-6Al-4V alloy [36]. With the temperature decrease further, the fractions of E13 and D14 reduce, while that of F14 continue to increase substantially. Until 1700 K, the fraction of F14 reaches 72%. since the F14 represents bcc structure, it can be inferred that the liquid Ti-6Al-4V alloy dominated by icosahedral-like structures (Fig. 6b) has crystallized into a bcc structure (Fig. 6c). The result is in good agreement with the results obtained from density, structure factor, PRDF, and BADF analyses.

3.6. Specific heat capacity

The specific heat capacity is one of the basic quantities discussed in the phase transition because it is a representative for the quantities of freedom and quite sensitive to structural change. The specific heat capacity C_v in FPMD simulations for the canonical ensemble can be calculated by the following equation [23,38],

$$C_v(T) = \frac{1}{k_B T^2}\left(\left\langle E^2\right\rangle - \langle E\rangle^2\right) \tag{5}$$

in which ⟨E⟩ is the average ensemble of free energy E and k_B is the Boltzmann constant.

In this section, an extra temperature, 1900 K, is added to research the specific heat capacity of Ti-6Al-4V alloy over the melting range. The calculated specific heat capacities at different temperatures are described in Table 1. In the high-temperature range of 2400–2000 K, the specific heat capacity increases slightly with decreasing temperature, which is

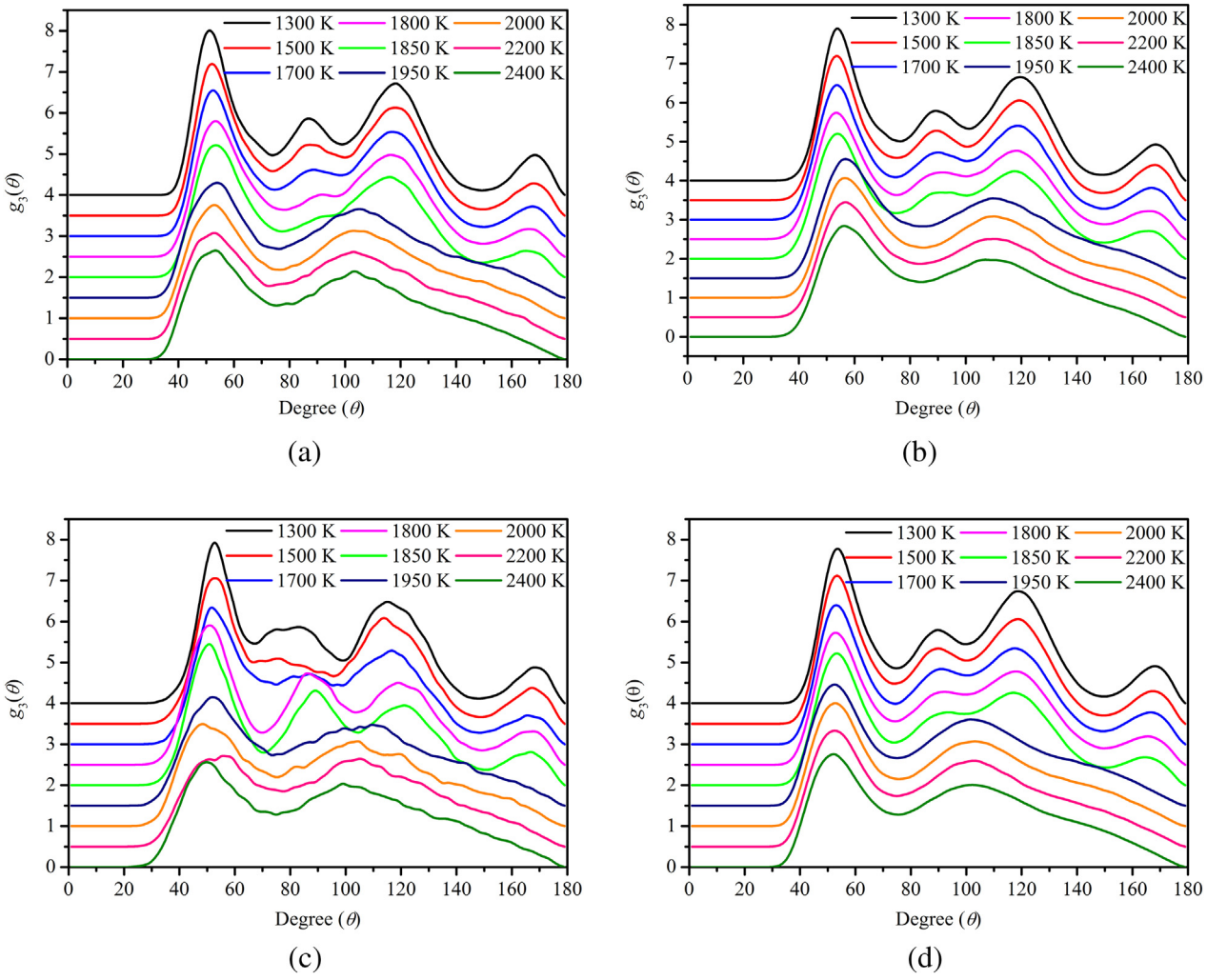

Fig. 5. The BADFs of (a) Ti-Al-Al, (b) Ti-Al-Ti, (c) Ti-Al-V, (d) Ti-Ti-Al, (e) Ti-Ti-Ti, (f) Ti-Ti-V, (g) Ti-V-Al, and (h) Ti-V-Ti triples at multiple temperatures. (Note that, for clarity, each curve has been vertically displaced from the curve below.)

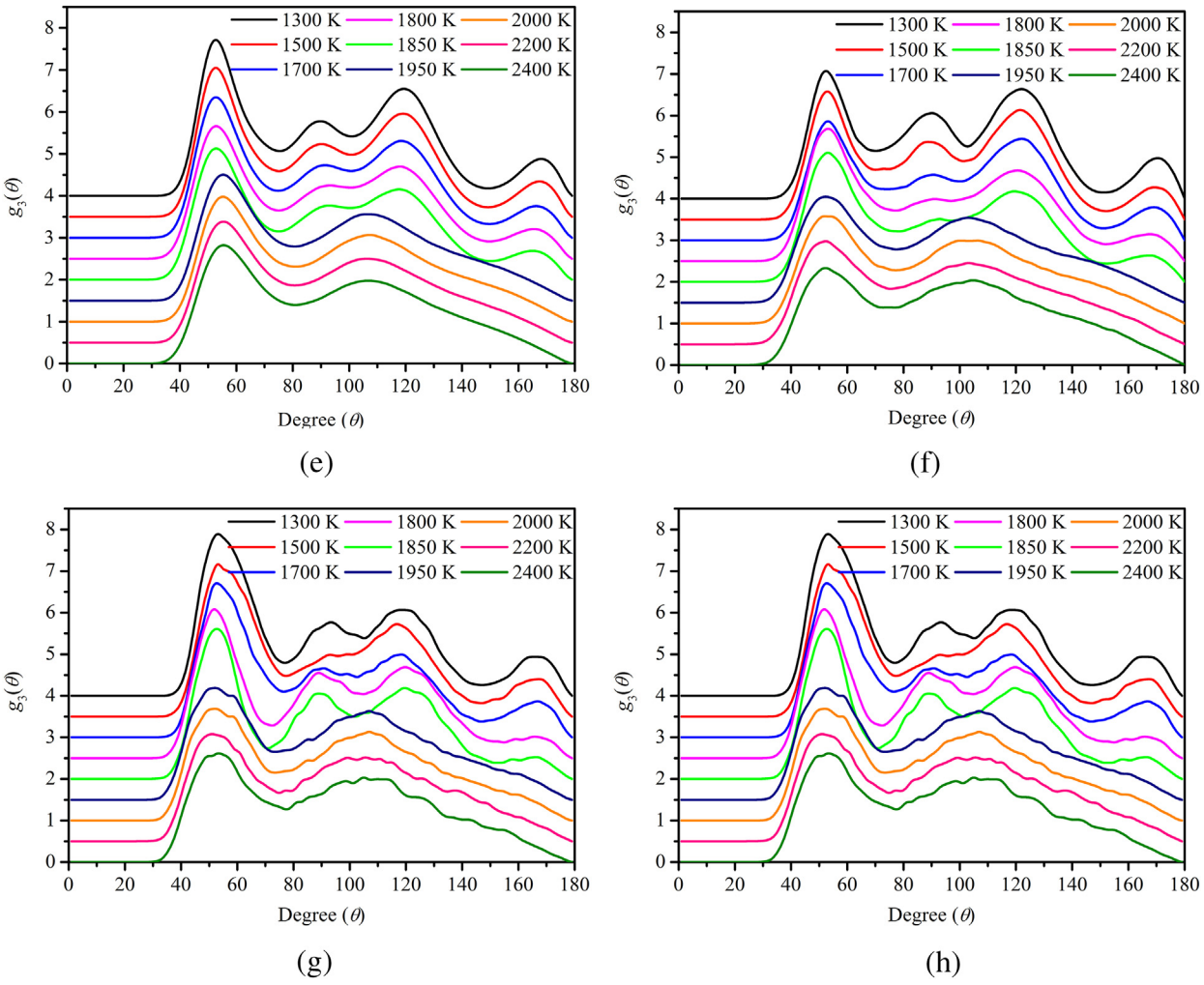

Fig. 5 (*continued*).

the normal behavior of an equilibrium liquid. In the temperature range of 1950–1850 K, a conspicuous endothermic peak of 2.200 $J \cdot g^{-1} \cdot K^{-1}$ is found at 1900 K. The similar trend is usually observed when a system takes place a phase transition, further meaning that temperature drops from 1950 K to 1850 K, the state of Ti-6Al-4V alloy changes from liquid to solid, which is in accordance with simulated density results. In the temperature range of 1800–1300 K, the specific heat capacity gradually increases with temperature increasing, which is a normal behavior of an equilibrium solid.

The experimental specific heat capacity reported by Kaschnitz et al. [39] is also summarized in Table 1 to verify our simulated values. Our FPMD specific heat capacities are less than experimental values with a max absolute error at 0.320 $J \cdot g^{-1} \cdot K^{-1}$ and a minimum absolute error at 0.250 $J \cdot g^{-1} \cdot K^{-1}$. Although the difference between the simulated and experimental value is quite large, the tendency of FPMD specific heat capacity with temperature coincides with the experimental value. Furthermore, the values measured from different experimental methods are quite different as well. For instance, the specific heat capacities at 1000 K are 0.960 $J \cdot g^{-1} \cdot K^{-1}$ (Basak et al.) [40], 0.736 $J \cdot g^{-1} \cdot K^{-1}$ (Milošević et al.) [41] and 0.745 $J \cdot g^{-1} \cdot K^{-1}$ (Kaschnitz et al.), respectively. The value of Basak differs from that of Milošević by 0.224 $J \cdot g^{-1} \cdot K^{-1}$, and that of Kaschnitz by 0.215 $J \cdot g^{-1} \cdot K^{-1}$. From these discussions, it can be concluded that experimental specific heat capacity differs greatly because the experimental measurement and theoretical calculation are prone to errors.

3.7. Diffusion coefficients

Additional information about structure evolution can be obtained by investigating the atom movement during solidification. For example, the dynamical properties of Ti-6Al-4V alloy are studied by calculating the mean-square displacement (MSD) as a function of time using the following equation,

$$\left\langle R_\alpha^2(t) \right\rangle = \frac{1}{N_\alpha} \left\langle \sum_{i=1}^{N_\alpha} |R_{i\alpha}(t+\tau) - R_{i\alpha}(\tau)|^2 \right\rangle \quad (6)$$

where N_α is the total atomic number of α species, $R_{i\alpha}$ is the coordinates of atom i, and τ is the arbitrary origin of time. The calculated MSD of each particle is shown in Fig. 7a-c. From the inset pictures in Fig. 7a-c, we find that the MSD of each particle oscillates around a mean value at different temperatures. As temperature varies from 1850 K to 1300 K, the mean values are 0.27, 0.31, 0.39, 0.46, and 0.49 $Å^2$ for Ti atom, 0.24, 0.28, 0.36, 0.43, and 0.48 $Å^2$ for Al atom, and 0.56, 0.56, 0.42, 0.34, and 0.30 $Å^2$ for V atom. These values suggest that in this temperature range, the thermal vibration of V atom is the largest, followed by Ti atom and finally Al atom. According to the transition state theory [42], the thermal vibration of atoms in a solid is proportional to the diffusion coefficient, thus, we can speculate that the order of diffusion coefficients is V > Ti > Al from 1850 K to 1300 K, which is compatible with the experimental results reported by Askill at el [43]. and Lee at el [44]..

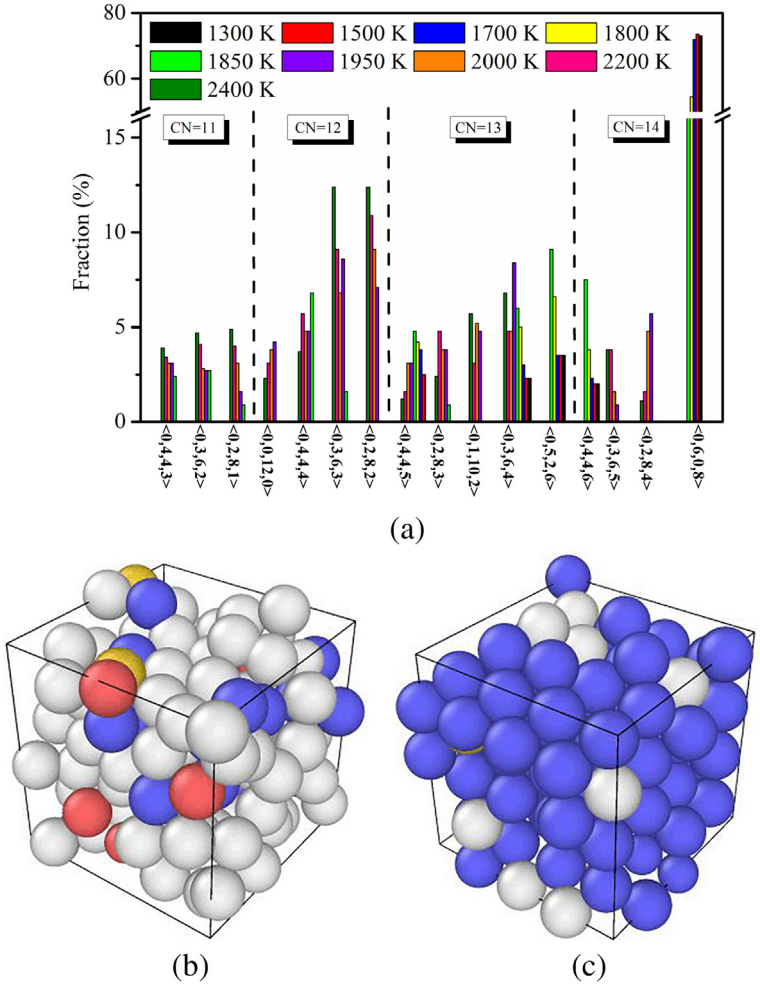

Fig. 6. (a) Fractions of main Voronoi indices in Ti-6Al-4V alloy at different temperatures and simulations snapshots at (b) 2400 K and (c) 1700 K. The atoms in snapshots are identified by common neighbor analysis with a standard visualization tool of OVITO, where the violet balls represent bcc structure, yellow balls represent perfect icosahedron, red balls represent hcp structure, and white balls represent other structure [37].

In addition, we also find that most MSD values at 1950 K, 2000 K, 2200 K, and 2400 K are greater 4 Å^2, while most MSD values at 1300 K, 1500 K,1700 K, 1800 K, and 1850 K are less than 4 Å^2. Some previous works demonstrate that the MSD values should be greater than 4 Å^2 to obtain statistically significant information on diffusivity, otherwise it will restrict the quantitative prediction of atomic diffusivity [35,45–47]. Thus, the MSD of 1950 K, 2000 K, 2200 K, and 2400 K are chosen for further analysis. The nearly linear dependence of MSD with time implies that Ti-6Al-4V alloy has already melted at each temperature and the equilibrium configurations are generated from our FPMD simulations. The inset pictures in Fig. 7a-c confirm the fact that the MSD oscillates around a mean value in a solid [9,48].

Table 1
Specific heat capacity (units: $J\cdot g^{-1}\cdot K^{-1}$) of Ti-6Al-4V alloy calculated from FPMD simulations together with experimental results.

T (K)	C_v (Calc.)	C_v (Expt.)
1300	0.434	0.733
1500	0.450	0.737
1700	0.477	0.775
1800	0.498	0.807
1850	0.506	0.826
1900	2.200	–
1950	0.700	–
2000	0.628	0.931
2200	0.623	0.931
2400	0.621	0.931

Note: The specific heat capacities at 1300 K and 1850 K are extrapolated from experimental values.

The diffusion coefficients D_α for Ti, Al, V atoms are evaluated from the slope of the MSD curve based on the Einstein relation,

$$D_\alpha = \lim_{n\to\infty}\left\langle R_{i\alpha}^2(t)\right\rangle/6t \tag{7}$$

The estimated diffusion coefficients for each species in liquid Ti-6Al-4V alloy at different temperatures are shown in Fig. 7d. As the temperature increases from 1950 to 2400 K, the diffusion coefficients increase from 4.46 to 7.02 × 10^{-5} cm^2s^{-1} for Ti, 3.89 to 6.62 × 10^{-5} cm^2s^{-1} for Al, and 5.53 to 8.17 × 10^{-5} cm^2s^{-1} for V, respectively, whose order of magnitude agrees with assumption reported by Semiatin et al. [49]. It can be found that the diffusion coefficient of V atom is the largest, followed by Ti atom, and finally the Al atom. This abnormal mass dependence of diffusion coefficient can be traced back to activation energy, which is obtained from the Arrhenius equation,

$$D_\alpha = D_0 e^{-E_\alpha/RT} \tag{8}$$

where E_α is the activation energy of α species, T is the temperature, D_0 is the pre-exponential factor, and R is the gas constant. From Fig. 7d, it is clearly seen that the diffusion coefficients for each particle satisfactorily

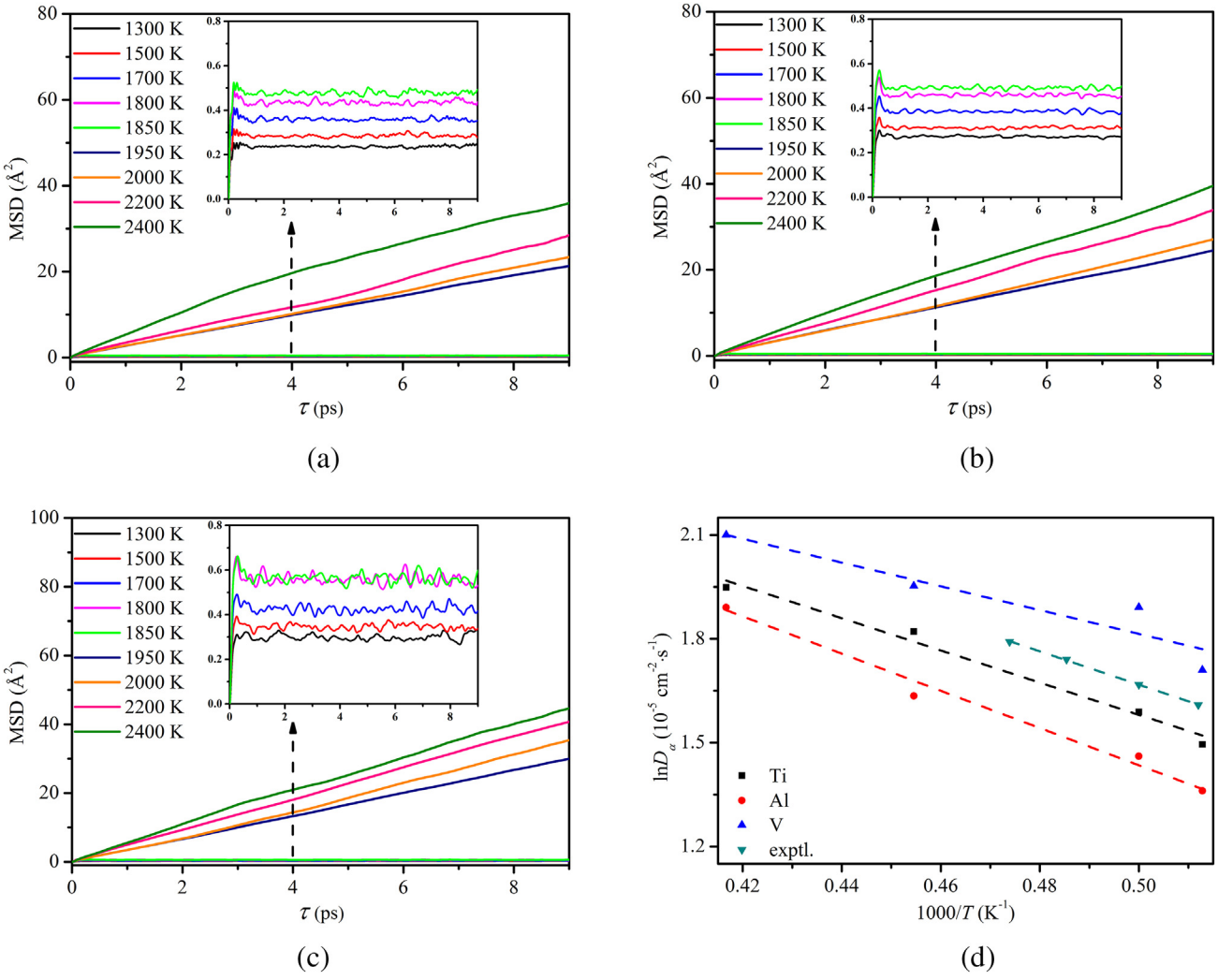

Fig. 7. The MSD of Al (a), Ti (b) and V (c) as a function of time at multiple temperatures and (d) temperature dependences of self-diffusion coefficients D_α for Ti, Al, and V.

comply with the Arrhenius relationship with R^2 values of 0.97 for Ti, 0.97 for Al and 0.81 for V. Fitting ln$D$ and $1/T$ to a linear function, the activation energies of Ti, Al, and V are obtained at 38.70, 44.69, and 28.55 kJ/mol, respectively. The smaller the activation energy, the faster the solute atom diffuse. Thus, the lower activation energy for V atom makes the V atom diffuse much faster than the other two atoms in the liquid Ti-6Al-4V alloy.

To our best knowledge, the diffusion coefficient in liquid Ti-6Al-4V alloy has not been measured by experiments or calculated by simulations, only the self-diffusion coefficient of a similar system, pure liquid Ti, was measured by the quasielastic neutron scattering method. The experimental values for Ti between (5.0 ± 0.1) and $(6.0 \pm 0.3) \times 10^{-5}$ cm^2s^{-1} in the temperature range of 1953–2110 K close to our simulated results [50]. Linearly fitting ln$D$ and $1/T$, the E_{Ti} in pure liquid Ti is calculated to be about 40.00 kJ/mol, which is smaller than the value of 52.8 kJ/mol in the pure liquid Ti predicted by Iida et al. [51] while slightly greater than our simulated E_{Ti} in liquid Ti-6Al-4V alloy.

3.8. Viscosity of liquid Ti-6Al-4V alloy

The shear viscosity, another key transport property describing liquid state dynamics, is calculated by the Stokes-Einstein-Sutherland equation from diffusion coefficients [15],

$$\eta = \frac{k_B T}{2\pi D_\alpha d_\alpha} \tag{9}$$

in which η is the shear viscosity of the liquid system, and d_α is the solvodynamic diameter of the diffusing atom. The diffusion coefficients of Ti have been calculated in Section 3.7 and the solvodynamic diameter of diffusing Ti atom is represented generally by averaging the first peak positions of $g_{Ti\text{-}Ti}(r)$, $g_{Ti\text{-}Al}(r)$ and $g_{Ti\text{-}V}(r)$ listed in Table 2. The viscosity estimated from the Stokes-Einstein-Sutherland equation is critically sensitive to the diffusion coefficients and first peak positions of PRDFs.

The inverse temperature dependence of viscosity obtained from the Stokes-Einstein-Sutherland equation is listed in Table 2 for liquid Ti-6Al-4V alloy. Viscosity calculated from FPMD simulations decreases with temperature increasing. In addition, the simulated viscosities are

Table 2
The first peak positions $R_{\alpha\beta}$ (Å), viscosity η (10^{-3} N·s·m^{-2}) of Ti-6Al-4V alloy in the temperature range of 1950–2400 K.

T	$R_{Ti\text{-}Ti}$	$R_{Ti\text{-}Al}$	$R_{Ti\text{-}V}$	$\overline{R}$	η
1950	2.843	2.796	2.702	2.820	3.408
2000	2.799	2.752	2.659	2.776	3.213
2200	2.811	2.764	2.672	2.787	2.806
2400	2.822	2.727	2.680	2.775	2.711

smaller than the value of 4.9×10^{-3} N·s·m^{-2} of pure Ti at 1923 K used by Mishra et al. [52], meaning that the addition of Al and V greatly reduces the viscosity of titanium alloy.

4. Conclusions

In this work, FPMD simulations are used to investigate the structural evolution and transport characteristics of Ti-6Al-4V alloy between 2400 K and 1300 K. The density calculated from FPMD simulations in NPT ensemble is remarkably close to the experimental value with absolute deviation between 0.09% and 0.80%, reflecting a good description of interatomic interaction in the Ti-6Al-4V alloys by PBE functional. Based on simulated density, the melting range of Ti-6Al-4V alloy is successfully predicted to be approximately 1850–1950 K, consistent well with experimental data.

After that, the trajectory of the system originated from the FPMD simulations is analyzed to research the structural evolution. Various structural analyses demonstrate that Ti-6Al-4V alloy experiences a phase transition from 2400 K to 1300 K. The system changes from a liquid dominated by icosahedral-like cluster to a solid with bcc structure, where the ⟨0, 5, 2, 6⟩ and ⟨0, 4, 4, 6⟩ polyhedra play an important role.

From the dynamical properties, it can be found that the diffusion coefficients of atoms in liquid Ti-6Al-4V alloy all obey Arrhenius function. The V atom has the largest diffusion coefficient, followed by the Ti atom, which is awfully close to the diffusion coefficient of pure liquid Ti, and finally the Al atom. This abnormal mass dependence of diffusion coefficient is well explained by activation energy.

To sum up, our results provide a deeper understanding of metallic solidification process on the atomic scale. More research to understand the correlation between the local structure and the electrical/mechanical properties in the cooling metallic liquids would be remarkably meaningful.

Declaration of competing interests

The authors declare that they have no known competing financial interests or personal relationships that could have appeared to influence the work reported in this paper.

CRediT authorship contribution statement

Jia Song: Conceptualization, Data curation, Formal analysis, Investigation, Methodology, Validation, Visualization, Writing - original draft, Writing - review & editing, Software.**Luyu Wang:**Validation, Investigation.**Liang Zhang:**Funding acquisition, Resources, Supervision. **Wenheng Wu:**Resources, Supervision.**Zhibin Gao:**Funding acquisition, Resources, Supervision.

Acknowledgments

This work is supported by the Shanghai Rising-star program (Project Number 18QB1400600). Z. Gao acknowledges financial support from MOE tier 1 funding of Singapore, Singapore (Grant No. R-144-000-402-114).

References

[1] P. Jia, J.Y. Zhang, X.Y. Teng, D.G. Zhao, Y. Wang, S. Hu, J. Xiang, S. Zhang, X. Hu, Liquid phase transition of $Sn_{50}Bi_{50}$ hypereutectic alloy and its thermodynamic and kinetic aspects, J. Mol. Liq. 251 (2018) 185–189.
[2] N. Kherrouba, D. Carron, M. Bouabdallah, R. Badji, Effect of solution treatment on the microstructure, micromechanical properties, and kinetic parameters of the $\beta \rightarrow \alpha$ phase transformation during continuous cooling of Ti-6Al-4V titanium alloy, J. Mater. Eng. Perform. 28 (2019) 6921–6930.
[3] J.H. Xia, Z.F. Cheng, D.P. Shi, X.Y. Xiao, A molecular dynamics study of structural transition of Ti during the rapid quenching process, Physica B 407 (2012) 2112–2118.
[4] Z.Y. Hou, R.S. Liu, Z.A. Tian, X. Wang, Q.Y. Zhou, Z.H. Chen, Formation mechanism of critical nucleus during nucleation process of liquid metal sodium, J. Chem. Phys. 127 (2007), 174503. .
[5] S.Y. Liu, Y.C. Shin, Additive manufacturing of Ti6Al4V alloy: a review, Mater. Des. 164 (2019), 107552. .
[6] L. Thijs, F. Verhaeghe, T. Craeghs, J.V. Humbeeck, J.P. Kruth, A study of the microstructural evolution during selective laser melting of Ti-6Al-4V, Acta Mater. 58 (2010) 3303–3312.
[7] M.F. Zhu, C.P. Hong, D.M. Stefanescu, Y.A. Chang, Computational modeling of microstructure evolution in solidification of aluminum alloys, Metall. Mater. Trans. B Process Metall. Mater. Process. Sci. 38 (2007) 517–524.
[8] L.H. Xiong, K. Chen, F.S. Ke, H.B. Lou, G.Q. Yue, B. Shen, F. Dong, S.Y. Wang, L.Y. Chen, C.Z. Wang, K.M. Ho, X.D. Wang, L.H. Lai, H.L. Xie, T.Q. Xiao, J.Z. Jiang, Structural and dynamical properties of liquid $Ag_{74}Ge_{26}$ alloy studied by experiments and ab initio molecular dynamics simulation, Acta Mater. 92 (2015) 109–116.
[9] T.T. Debela, X.D. Wang, Q.P. Cao, D.X. Zhang, S.Y. Wang, C.Z. Wang, J.Z. Jiang, Atomic structure evolution during solidification of liquid niobium from *ab initio* molecular dynamics simulations, J. Phys. Condens. Matter 26 (2013) 055004.
[10] N. Jakse, A. Pasturel, Transport properties and Stokes-Einstein relation in Al-rich liquid alloys, J. Chem. Phys. 144 (2016), 244502. .
[11] B. Zhang, X.Y. Zhang, C. Li, K.C. Zhou, Molecular dynamics simulation on phase transformation of Ti-Al alloy with low Al content, Rare Metal Mat. Eng. 41 (2012) 1010–1105.
[12] M. Shimono, H. Onodera, Molecular dynamics study on formation and crystallization of Ti-Al amorphous alloys, Mater. Sci. Eng. A 304 (2001) 515–519.
[13] T. Fujinaga, Y. Watanabe, Y. Shibuta, Nucleation dynamics in Al solidification with Al-Ti refiners by molecular dynamics simulation, Comput. Mater. Sci. 182 (2020) 109763.
[14] P.T. Li, Y.Q. yang, W. Zhang, X. Luo, N. Jin, G. Liu, Structural evolution of TiAl during rapid solidification processing revealed by molecular dynamics simulations, RSC Adv. 6 (2016) 54763–54767.
[15] J. Song, S.P. Shi, X.J. Li, L.M. Yan, First-principles molecular dynamics modeling of UCl_3 in LiCl-KCl eutectic, J. Mol. Liq. 234 (2017) 279–286.
[16] Y. Zhang, J. Song, X.J. Li, L.M. Yan, S.P. Shi, T. Jiang, S.M. Peng, First principles calculation of redox potential for tetravalent actinides in molten LiCl-KCl eutectic based on vertical substitution and relaxation, Electrochim. Acta 293 (2019) 466–475.
[17] G. Kresse, J. Hafner, *Ab initio* molecular dynamics for liquid metals, Phys. Rev. B 47 (1993) 558.
[18] G. Kresse, J. Furthmüller, Efficient iterative schemes for *ab initio* total-energy calculations using a plane-wave basis set, Phys. Rev. B 54 (1996), 11169. .
[19] J.P. Perdew, K. Burke, M. Ernzerhof, Generalized gradient approximation made simple, Phys. Rev. Lett. 77 (1996) 3865.
[20] J.P. Perdew, K. Burke, Comparison shopping for a gradient-corrected density functional, Int. J. Quant. Chem. 57 (1996) 309–319.
[21] G. Kresse, D. Joubert, From ultrasoft pseudopotentials to the projector augmented-wave method, Phys. Rev. B 59 (1999) 1758.
[22] P.E. Blöchl, Projector augmented-wave method, Phys. Rev. B 50 (1994), 17953. .
[23] L.H. Xiong, X.D. Wang, Q. Yu, H. Zhang, F. Zhang, Y. Sun, Q.P. Cao, H.L. Xie, T.Q. Xiao, D.X. Zhang, C.Z. Wang, K.M. Ho, Y. Ren, J.Z. Jiang, Temperature-dependent structure evolution in liquid gallium, Acta Mater. 128 (2017) 304–312.
[24] J.J.Z. Li, W.L. Johnson, W.K. Rhim, Thermal expansion of liquid Ti-6Al-4V measured by electrostatic levitation, Appl. Phys. Lett. 89 (2006) 111913.
[25] S. Melchionna, G. Ciccotti, B.L. Holian, Hoover NPT dynamics for systems varying in shape and size, Mol. Phys. 78 (1993) 533–544.
[26] Y. Cheng, Y.Y. Wang, C.X. Peng, Z.T. Zhang, P.F. Wang, L.J. Jia, X.L. Li, L. Wang, Dynamic and structural heterogeneity in undercooled miscible and immiscible metallic liquid, J. Alloy. Compd. 786 (2019) 627–635.
[27] M. Boivineau, C. Cagran, D. Doytier, V. Eyraud, M.H. Nadal, B. Wilthan, G. Pottlacher, Thermophysical properties of solid and liquid Ti-6Al-4V (TA6V) alloy, Int. J. Thermophys. 27 (2006) 507–529.
[28] Q. Yu, F.M. Guo, X.D. Wang, K. Ståhl, Y. Ren, Q.P. Cao, D.X. Zhang, J.Z. Jiang, Structural evolution of low-temperature liquid GaIn eutectic alloy, J. Mol. Liq. 293 (2019), 111464. .
[29] A. Pasturel, N. Jakse, Influence of Cr on local order and dynamic properties of liquid and undercooled Al-Zn alloys, J. Chem. Phys. 146 (2017), 184502. .
[30] T.T. Debela, X.D. Wang, Q.P. Cao, D.X. Zhang, J.J. Zhu, J.Z. Jiang, Phase selection during solidification of liquid magnesium via *ab initio* molecular dynamics simulations, J. Appl. Phys. 117 (2015), 114905. .
[31] Y. Su, M. Mohr, R.K. Wunderlich, X.D. Wang, Q.P. Cao, D.X. Zhang, Y. Yang, H.J. Fecht, J.Z. Jiang, The relationship between viscosity and local structure in liquid zirconium via electromagnetic levitation and molecular dynamics simulations, J. Mol. Liq. 298 (2020), 111992. .
[32] W.Y. Wang, J.J. Han, H.Z. Fang, J. Wang, Y.F. Liang, S.L. Shang, Y. Wang, X.J. Liu, L.J. Kescskes, S.N. Mathaudhu, X. Hui, Z.K. Liu, Anomalous structural dynamics in liquid $Al_{80}Cu_{20}$: an *ab initio* molecular dynamics study, Acta Mater. 97 (2015) 75–85.
[33] H.W. Sheng, W.K. Luo, F.M. Alamgir, J.M. Bai, E. Ma, Atomic packing and short-to-medium-range order in metallic glasses, Nature 439 (2006) 419–425.
[34] Z.Z. Wu, Y.F. Mo, L. Lang, A.B. Yu, Q. Xie, R.S. Liu, Z.A. Tian, Topologically close-packed characteristic of amorphous tantalum, Phys. Chem. Chem. Phys. 20 (2018) 28088–28104.
[35] J.J. Han, W.Y. Wang, X.J. Liu, C.P. Wang, X.D. Hui, Z.K. Liu, Effect of solute atoms on glass-forming ability for Fe-Y-B alloy: an *ab initio* molecular dynamics study, Acta Mater. 77 (2014) 96–110.
[36] S.P. Pan, S.D. Feng, J.W. Qiao, W.M. Wang, J.Y. Qin, Crystallization pathways of liquid-bcc transition for model iron by fast quenching, Sci. Rep. 5 (2015) 16956.
[37] A. Stukowski, Visualization and analysis of atomistic simulation data with OVITO-the open visualization tool, Modelling Simul, Mater. Sci. Eng. 18 (2010) 015012.

[38] X.W. Fang, C.Z. Wang, Y.X. Yao, Z.J. Ding, K.M. Ho, Atomistic cluster alignment method for local order mining in liquids and glasses, Phys. Rev. B 82 (2010), 184204. .
[39] E. Kaschnitz, P. Reiter, J.L. McClure, Thermophysical properties of solid and liquid 90Ti-6Al-4V in the temperature range from 1400 to 2300 K measured by millisecond and microsecond pulse-heating techniques, Int. J. Thermophys. 23 (2002) 267–275.
[40] D. Basak, R.A. Overfelt, D. Wang, Measurement of specific heat capacity and electrical resistivity of industrial alloys using pulse heating techniques, Int. J. Thermophys. 24 (2003) 1721–1733.
[41] N. Milošević, I. Aleksić, Thermophysical properties of solid phase Ti-6Al-4V alloy over a wide temperature range, Int. J. Mater. Res. 103 (2012) 707–714.
[42] R. Gomer, Diffusion of absorbates on metal surface, Rep. Prog. Phys. 53 (1990) 917–1002.
[43] J. Askill, G.B. Gibbs, Tracer diffusion in β-titanium, Phys. Status Solidi B 11 (1965) 557–565.
[44] S.Y. Lee, O. Taguchi, Y. Iijima, Diffusion of aluminum in β-titanium, Mater. Trans. 51 (2010) 1809–1813.
[45] H.S. Lee, M.E. Tuckerman, Dynamical properties of liquid water from ab initio molecular dynamics performed in the complete basis set limit, J. Chem. Phys. 126 (2007), 164501. .
[46] D. Alfè, C. Cazorla, M.J. Gillan, The kinetics of homogeneous melting beyond the limit of superheating, J. Chem. Phys. 135 (2011), 024102. .
[47] W.Y. Wang, H.Z. Fang, S.L. Shang, H. Zhang, Y. Wang, X. Hui, S. Mathaudhu, Z.K. Liu, Atomic structure and diffusivity in liquid $Al_{80}Ni_{20}$ by *ab initio* molecular dynamics simulations, Physica B 406 (2011) 3089–3097.
[48] H. Li, G.H. Wang, X.F. Bian, F. Ding, Local cluster formation in a cobalt melt during the cooling process, Phys. Rev. B 65 (2001) 035411.
[49] S.L. Semiatin, V.G. Ivanchenko, O.M. Ivasishin, Diffusion models for evaporation losses during electron-beam melting of alpha/beta-titanium alloys, Metall. Mater. Trans. B Process Metall. Mater. Process. Sci. 35 (2004) 235–245.
[50] J. Horbach, R.E. Rozas, T. Unruh, A. Meyer, Improvement of computer simulation models for metallic melts via quasielastic neutron scattering: a case study of liquid titanium, Phys. Rev. B 80 (2009), 212203. .
[51] T. Iida, R. Guthrie, N. Tripathi, A model for accurate predictions of self-diffusivities in liquid metals, semimetals, and semiconductors, Metall. Mater. Trans. B Process Metall. Mater. Process. Sci. 37 (2006) 559–564.
[52] S. Mishra, T. DebRoy, Measurements and Monte Carlo simulation of grain growth in the heat-affected zone of Ti-6Al-4V welds, Acta Mater. 52 (2004) 1183–1192.